Asociación Argentina
de Mecánica Computacional

Mecánica Computacional Vol XXXI, págs. 211-235 (artículo completo)
Alberto Cardona, Paul H. Kohan, Ricardo D. Quinteros, Mario A. Storti (Eds.)
Salta, Argentina, 13-16 Noviembre 2012

A NUMERICAL MODEL FOR POLLUTANT DISPERSION SIMULATION IN STREET CANYONS

Deborah M. S. Madalozzo, Alexandre L. Braun and Armando M. Awruch

PPGEC/UFRGS, Graduate Program in Civil Engineering, Federal University of Rio Grande do Sul, Av. Osvaldo Aranha 99, 90035-190, Porto Alegre – RS, Brazil, http://www.ufrgs.br/engcivil/ppgec/

Keywords: Computational Fluid Dynamics (CFD), Finite Element Method (FEM), Pollutant Dispersion, Non-Isothermal Flow, Large Eddy Simulation (LES).

Abstract. In this work, pollutant dispersion analyses in urban areas are carried out employing a model developed for numerical simulation of incompressible flows considering the effects of heat and mass transfer. Air pollution generated by vehicles with internal combustion engines is one of the biggest problems the large cities are facing today. Therefore, the development of numerical techniques for evaluating and controlling the levels of pollutants is essential to maintain the urban environment balance. In the central regions of large cities, the so-called street canyons represent the basic geometric unit, where significant changes can be observed in the wind flow and pollutant dispersion as function of thermal conditions and the geometrical configuration of the canyons. In the present model, an explicit two-step Taylor-Galerkin scheme is adopted where the spatial discretization is performed using the finite element method (FEM) with eight-node hexahedral elements, one-point quadrature and hourglass control techniques. The pressure field is explicitly obtained by using the pseudo-compressibility hypothesis and the velocity and temperature fields are coupled by buoyancy forces according to the Boussinesq approximation. Large eddy simulation (LES) is utilized to analyze turbulent flows, where the sub-grid scales are modeled using both, the classical Smagorinsky`s model and the dynamic model. Applications involving isothermal and non-isothermal flows are reproduced in order to validate the numerical model presented here and isothermal pollutant dispersion problems are simulated considering different geometrical configurations represented by two and three-dimensional models in order to adequately characterize the conditions encountered in urban areas.

1 INTRODUCTION

The environmental conditions in large cities have been constantly deteriorated during the last decades owing to pollutants emitted by motor vehicles. Government agencies for air pollution control have adopted some procedures in order to reduce the pollutant emissions, which are mainly based on data obtained from monitoring stations strategically located to quantify the air quality in terms of pollutant concentration. However, the number of monitoring stations is clearly insufficient to describe the distribution of pollutants over the streets accurately. In addition, air flow and pollutant dispersion through the streets of large cities are very complex, including aerodynamic and transport phenomena, where thermal effects play an important role. Among the available techniques to reproduce urban street flows, Computational Fluid Dynamics (CFD) has attracted special attention owing to significant improvements observed in the field of turbulence modeling and rapid advances verified in processing power and storage capacity of computational systems. Nevertheless, numerical simulation requires careful validation against reference results, which may be obtained from field measurements, experimental evaluations in wind tunnels or parametric studies performed with different numerical models.

In the present work, an overview on the subject of pollutant dispersion in urban areas is presented, where the main aspects related to flow and transport phenomena in street canyons are analyzed in order to define the most important topics for the development of reliable CFD models. A numerical model based on the Finite Element Method (FEM) and Large Eddy Simulation (LES) is also proposed in order to investigate pollutant dispersion in street canyons with thermal effects. The basic formulation adopted in the present model was previously validated for applications on building aerodynamics (see Braun and Awruch, 2009a), which is extended here to include mass and heat transport phenomena in the flow analysis. In this work, applications involving isothermal and non-isothermal flows are reproduced in order to validate the numerical model proposed here and isothermal pollutant dispersion problems are studied using two and three-dimensional street canyon models.

1.1 Flow field in urban street canyons

The flow field in urban areas is mainly influenced by geometrical and meteorological aspects such as building shape, street width, wind speed and direction, turbulence, solar radiation and photochemical reactions (Kim and Baik, 1999). By analyzing the downtown area of large cities, one can identify a basic geometric configuration composed of long streets laterally confined by medium-rise and high-rise buildings, where the canyon effect is frequently observed. Therefore, experimental and numerical investigations have been performed considering this representative configuration of the urban street geometry, which is commonly defined as urban street canyon (Nicholson, 1975). In the street canyons, the wind flow presents shear layer characteristics, with vortices usually generated at the leading edge of the canyon cavity and impingement observed on the trailing edge. In addition, recirculation regions and complex wake structures are also noticed. The urban canopy layer is vertically enclosed by the street surface and the roof level of the surrounding buildings, where microscale meteorological effects are significant. Moreover, large amounts of pollutants are released near the ground from motor vehicles and along the height of the buildings from domestic and industrial exhaust systems. Thermal effects are also observed, which are induced by solar radiation absorbed by building walls and ground surface. Therefore, the major parameters affecting pollutant transport are flow conditions, building and street geometry, thermal stratification and vehicle movement. Some comprehensive reviews on

street canyon flows may be found in Vardoulakis et al. (2003), Ahmad et al. (2005), Li et al. (2006) and Hajra (2011).

One of the first studies especially dedicated to street canyon flows is due to Oke (1988), who determined flow regimes based on experimental analyses performed with different aspect ratios (AR) (ratio of the building height to the width between buildings). The flow regimes were classified into isolated roughness flow, wake interference flow and skimming flow. However, the study carried out by Oke (1988) did not take into account effects of Reynolds number and pollutant dispersion. Another important aspect that was not considered is the thermal effect over transport phenomena.

Street canyons are closely related to the cavity flow problem, which has been extensively investigated by the CFD community (see, for instance, Ghia et al, 1982; Tang et al., 1995; Leriche and Gavrilakis, 2000). However, in the case of street canyons, communication between the cavity and main flow may be observed depending on the canyon geometry. When the buildings composing the street canyon are widely spaced ($AR < 0.3$), isolated roughness flow is obtained, since no interaction is noticed between the flow fields generated on the buildings individually (see Oke, 1988). By reducing the building spacing ($0.3 < AR < 0.7$), the recirculation zone created by the upwind building is modified by the action of the recirculation zone generated by the downwind building, which leads to the wake interference flow regime. For aspect ratio $AR \approx 1$, a stable vortex is usually obtained with secondary vortices located at the bottom corners of the canyon and the main flow is decoupled from the street flow. For aspect ratio $1 < AR < 3$, two stable vortices are identified inside the canyon cavity, where a vertically aligned configuration with counter-rotating recirculation is observed. Numerical investigations on the flow field inside street canyons with different AR may be found in Lee and Park (1994), Sini et al. (1996), Baik and Kim (1999), Chan et al. (2002) and Jeong and Andrews (2002), where two-dimensional models were adopted.

Numerical investigations are frequently performed considering two-dimensional models, which are usually justified by taking into account that the two-dimensional approach could represent flows in street canyons with infinite length along the span-wise direction. Moreover, computational efforts are significantly reduced when two-dimensional simulations are carried out. However, street-canyon flows are essentially three-dimensional, since high Reynolds numbers are generally obtained. In addition, some flow phenomena such as horseshoe vortices and lateral eddy circulation associated with wake and interference flows cannot be reproduced when the two-dimensional approach is adopted. Some of these flow structures were described by Baik and Kim (1999), who observed that these aspects play an important role in pollutant dispersion around buildings and, therefore, they require three-dimensional models to analyze the flow and transport problems adequately.

In order to reproduce the street canyon problem realistically, street intersections must be also considered. One can notice that complicated flow patterns are observed at the intersection region, where dispersion and mixing of pollutants are strongly influenced by the geometric configuration of the street intersection. Some recent works have been devoted to numerically study the effects of street intersections over airflow and pollutant dispersion in urban areas. Effects of crossroad intersections over the street canyon flow were studied by Chan et al. (2003). More recently, Yassin et al. (2008) investigated the influence of different street intersection shapes on flow and pollutant transport in street canyons and Soulhac et al. (2009) compared experimental and numerical predictions by using a simple geometrical configuration composed of hexahedral buildings and orthogonal intersection streets.

1.2 CFD and turbulence modeling

CFD has become one of the most popular and reliable techniques to analyze real applications involving complex wind flow phenomena (see, for instance, Braun and Awruch, 2008; Braun and Awruch, 2009a; Braun and Awruch, 2009b). This success can be attributed to three main reasons: constant improvements in computer technology, development of high accuracy numerical methods, especially turbulence models, and more recently, popularization of parallel computing techniques. Consequently, Computational Wind Engineering (CWE) is now a major topic for experts on CFD (see Blocken, 2011), where pollutant dispersion in street canyons is one of the subjects investigated.

Some methods have been utilized to study the street canyon problem, such as field measurements and wind tunnel experiments (see, for instance, Kastner-Klein and Plate, 1999; Pavageau and Schatzmann, 1999; Xie et al., 2003), but only numerical simulations performed with CFD models can really provide results with high resolution, where comprehensive information on the flow field can be found from flow variables evaluated at any point of the computational domain and for any instant in time. In addition, problems can be analyzed at full scale and parametric studies are easily carried out by simply changing geometrical and physical constants that define the numerical model.

Nevertheless, numerical simulation using CFD techniques requires special care in order to obtain reliable results, which may be verified through grid sensitivity analysis, parametric studies or experimental validation. The accuracy of predictions obtained from CFD models are mainly influenced by grid resolution and numerical procedures related to turbulence modeling. Moreover, when CFD models are applied to problems of heat and mass transfer in turbulent flows, additional parameters must be defined, such as the turbulent Prandtl number (Prt) and the turbulent Schmidt number (Sct). Reynolds (1975) investigated the turbulent Prandtl number and the turbulent Schmidt number, who concluded that the sub-grid scale (SGS) Schmidt number is not constant, but varies with the molecular Schmidt number and the distance to solid walls, where anisotropic behavior is observed. The same remark is applied to the turbulent Prandtl number, where higher values are found near walls and approximately constant distribution is observed away from walls.

Numerical models have generally adopted constant values for the turbulent Schmidt and Prandtl numbers, which is similar to assume isotropic behavior in the sub-grid scales. As stated before, this assumption is not valid for flow regions near walls. Therefore, refined meshes are required in order to obtain reliable results in these regions. Due to the lack of a deep insight about this matter, CFD simulations have been carried out using several Prt and Sct numbers to validate the numerical models against reference results. A numerical investigation on Schmidt numbers for CFD analysis was recently presented by Tominaga and Stathopoulos (2007), where it is recommended to determine Sct according to the flow characteristics observed in each case. However, conclusions demonstrated that the turbulent Schmidt number may be used to make up deficiencies of the k-ε turbulence model. Large Eddy Simulation (LES) was not addressed in their studies.

Numerical simulation of wind flow and pollutant dispersion in street canyons is highly dependent on the turbulence model adopted owing to the turbulent nature of the wind flow around buildings. The first numerical investigations on street canyon flows were carried out using RANS (Reynolds Averaged Navier-Stokes), where steady-state solutions are obtained using coarse meshes. However, it is well known from CWE that RANS schemes with the k-ε model cannot reproduce most of the flow phenomena observed in bluff body aerodynamics (see Murakami, 1997). Although some modifications were proposed in order to improve

results obtained with the standard k-ε model, such as the RNG k-ε model (Yakhot and Orszag, 1986), the k-ω model (Wilcox, 1988) and the realizable k-ε model (Shih et al., 1995), they are still far away from the level of accuracy achieved by LES models. In recent papers, Tominaga and Stathopoulos (2010, 2011), Santiago et al. (2010) and Gosseau et al. (2010) compared CFD predictions obtained with LES and RANS for pollutant dispersion around buildings in street canyons. The authors reported that RANS computations are less accurate when compared with results provided by LES models, which usually present good agreement with experimental predictions.

Special attention has been given recently to LES in order to overcome the shortcomings presented by RANS models in street canyon flows. LES was traditionally avoided in many CFD applications because SGS modeling requires highly refined meshes near the solid walls in order to obtain accurate results. Nevertheless, most of those applications can be simulated now using LES with standard computer configurations. LES is able to calculate a significant range of the flow turbulent scales straightforwardly, while effects of the sub-grid scales over the large scales are approximated using turbulence modeling. The standard Smagorinsky's SGS model (Smagorinsky, 1963) has been applied to applications on pollutant dispersion in street canyons, where the empirical constant CS (Smagorinsky's constant), which is referred to the SGS eddy viscosity model, is usually set to 0.12. The Smagorinsky's constant can be evaluated dynamically by using the numerical procedure proposed by Germano et al. (1991) and Lilly (1992). However, it is observed that the dynamic model frequently leads to numerical instability owing to the large range of fluctuations verified in the Smagorinsky's parameter. In addition, some difficulties associated with the near-wall behavior have been reported (see Iizuka and Kondo, 2004). In order to circumvent these drawbacks, the Lagrangian dynamic model and wall functions may be adopted (see Meneveau et al., 1996; Piomelli, 2008).

The first numerical simulations of pollutant dispersion in street canyons using LES are due to Ca et al. (1995) and Chabni et al. (1998), where two-dimensional approaches and classical Smagorinsky's SGS models were adopted. Walton et al. (2002) and Walton and Cheng (2002) utilized LES and the dynamic SGS model to analyze three-dimensional street canyons. The dynamic SGS model was also employed by Liu and Barth (2002) and Liu et al. (2004, 2005) to investigate three-dimensional flow fields and pollutant transport in street canyons with different aspect ratios and Reynolds number of 1.2x104. LES and the Smagorinsky's SGS model were used by Cui et al. (2004) to simulate the street canyon problem considering three-dimensional configurations with aspect ratio AR = 1 and large Reynolds number. So et al. (2005) investigated several street canyon configurations for different Reynolds number using three-dimensional LES and the classical Smagorinsky's SGS model. In Li et al. (2008), a LES model was developed to investigate the flow field and pollutant dispersion for street canyons with high AR. The Smagorinsky' model was utilized for sub-grid modeling and a wall model was implemented in order to reduce refinement requirements near walls. More recently, LES has been adopted to study dispersion of reactive pollutants in street canyons (see Baker et al. 2004; Grawe et al., 2007; Kikumoto and Ooka, 2011).

1.3 Air Pollution dispersion

The main sources of air pollution in urban areas are due to combustion products emitted from motor vehicles with propulsion systems based on fossil fuels. Consequently, the following traffic-related air pollutants can be identified in street canyons: carbon monoxide CO, carbon dioxide CO_2, sulfur dioxide SO_2, nitrogen oxides NO_x (NO_2 – nitrogen dioxide;

NO – nitrogen monoxide), hydrocarbon volatile organic compounds VOC (propane, ethylene, toluene, xylene, benzene, butane, ethane, pentane, etc.), suspended particulate matter (PM) and aerosols. The main derivatives of the combustion process are CO_2, water and PM. CO is obtained as a product of imperfect fuel combustion and a mixture of NO_x is produced from the reaction of nitrogen and oxygen gases present in the air, which is induced by high temperatures observed in the combustion chamber of engines (see Vardoulakis et al., 2003). It is verified that more than 90% of the resulting NO_x is found in the form of NO. These species can chemically react in the presence of sunlight (photolysis reaction), producing secondary pollutants such as ozone O_3 and aerosols. Some of the pollutants primarily emitted by combustion can react with atmospheric oxidants or each other to produce other secondary products. Particles of condensed carbonaceous material are emitted mainly by diesel and motor vehicles with inadequate maintenance. Large fractions of fine PM are also produced by chemical oxidation of gases obtained from primary emissions, such as SO_2 and NO_x, and the subsequent gas-to-particle conversion. Several chemically transformed hydrocarbons are also emitted by motor vehicles through processes such as evaporation and fuel tank displacement (see Vardoulakis et al., 2003).

Most of the traffic-related pollutants in urban areas can be considered as inert species, since pollutant concentration is only influenced by fast chemical reactions due to the short distances observed between sources and receptors within the street canyons (Berkowicz et al., 1997). Considering that NO_2 dissociates extremely fast in the presence of light and NO also reacts very fast with O_3 (Palmgren et al., 1996), these are the reactive gases usually included in transport models for pollutant dispersion. While the time scales associated with these chemical reactions are comparable with the time scales of the pollutant transport in street canyons, effects induced by chemical reaction should be considered in the mass transport model. Other chemical reactions are expected to have little influence on the spatial distribution of the pollutant concentration within street canyons, since they are usually associated with much slower timescales. Photochemical processes are very important for models of pollutant dispersion, since urban chemistry is very sensitive to photolysis reactions (Carter, 1994). Carpenter et al. (1998) observed that the photostationary state is usually obtained after one or two minutes when the reactive gases are submitted to typical daytime conditions.

In most of the numerical studies performed so far, pollutant dispersion through street canyons has been determined considering only passive pollutants, where chemical reactions are not included in the transport equations. Owing to computational limitations, many of the chemical reactions occurring with atmospheric species cannot be represented. Therefore, simplified models have been introduced recently in order to obtain a representative scheme of the photochemical phenomena observed in the urban environment (Dodge, 2000). The first investigation on transport of reactive pollutants in urban street canyons was performed by Baker et al. (2004), where a simplified model for steady state O_3-NO-NO_2 photochemistry is utilized. Baik et al. (2007) extended the model adopted by Baker et al. (2004) to account for temperature-dependent reactions. Dispersion of reactive pollutants in street canyons under turbulent flow was investigated by authors such as Grawe et al. (2007) and Kang et al. (2008), where steady state O_3-NO-NO_2 photochemistry was also adopted. On the other hand, more complex chemical mechanisms have been proposed. Liu and Leung (2008) developed a numerical model to simulate pollutant dispersion considering photochemical reactions with important O_3 precursors such as reactive VOCs. Production and dispersion of PM in urban street canyons were simulated by Gidhagen et al. (2005) and Kumar et al. (2008a, b) and chemistry schemes comprising several species were utilized by Garmory et al. (2009) and

Kwak and Baik (2012) in their numerical investigations on pollutant dispersion in the urban environment.

1.4 Thermal effects

The building walls and street surfaces composing the urban canyon are heated owing to the incidence of solar radiation, which leads to the development of upward buoyancy forces over the flow field (see Kim and Baik, 2001; Louka and Vachon, 2001). The buoyancy forces induced by solar radiation may be significant, especially for wind flows with low speeds, since large temperature differences are usually observed in the street canyons. It is important to notice that buildings and streets are mostly made of concrete and asphalt, which are materials with low heat capacity (see Sakakibara, 1996). Additional parameters influencing solar heating in street canyons are orientation, albedo, emissivity of the building and street materials, and the sky view factor.

Some numerical studies on buoyant flow in street canyons have been carried out in the last decades. In Sini et al. (1996) and Kim and Baik (1999), flow and pollutant transport in two-dimensional canyon configurations with several aspect ratios are investigated considering buoyant forces induced by differential heating of the street surfaces. Results demonstrated that wall temperature can significantly influence the flow structure and the vertical transport in the street canyon. The same findings were reported by Xie et al. (2005, 2006), where RANS and the k-ε turbulence model were also adopted to analyze two-dimensional canyon configurations. Sakakibara (1996) obtained numerical predictions for street canyon flows showing that the urban thermal environment depends on urban geometry when reduced sky view factors and complicated daytime shadow patterns are considered. Street canyon flows with thermal effects were investigated by Baik et al. (2003) using a three-dimensional RANS model. LES was initially employed to simulate two-dimensional street canyon flows under thermal stratification in the work presented by Ca et al. (1995). Two-dimensional LES models were also utilized recently by Li et al. (2009) and Cheng and Liu (2011) to analyze effects of ground heating and thermal stratification on the pollutant transport in urban canyons. Many of these numerical models have been validated using the experimental results presented by Uehara et al. (2000).

2 MODEL DESCRIPTION

2.1 Flow and transport equations

The flow problem in urban street canyons is mathematically described using balance equations for momentum, mass and energy, and the scalar transport equation for pollutant species. Some hypothesis may be considered in order to simply the general formulation. In the present work, the same assumptions adopted by Braun and Awruch (2009a) to characterize wind flows are utilized and additional hypotheses are also specified regarding the pollutant transport. The main postulates assumed in the present model may be summarized as follows:

(a) Wind flows are assumed to be incompressible;

(b) Air density is assumed to be constant;

(c) Air density variations due to temperature effects are considered only in terms of buoyancy forces acting on the momentum equations;

(d) Pollutant species are assumed to be mechanically passive and chemically inert;

(e) The Newtonian fluid model is adopted for constitutive description of the air.

The governing equations are kinematically described using the classical Eulerian approach and the mass balance equation is written here according to the pseudo-compressibility hypothesis (see Braun and Awruch, 2009a), which leads to flow formulations where the pressure field is obtained explicitly. Considering the Cartesian coordinate system, the flow governing equations for street canyon flows may be presented as follows:

Momentum equations – the Navier-Stokes equations:

$$\frac{\partial v_i}{\partial t}+v_j\frac{\partial v_i}{\partial x_j}=\frac{\partial}{\partial x_j}\left[\nu\left(\frac{\partial v_i}{\partial x_j}+\frac{\partial v_j}{\partial x_i}\right)+\frac{\lambda}{\rho}\frac{\partial v_k}{\partial x_k}\delta_{ij}\right]+\frac{1}{\rho}\left(S_i-\frac{\partial p}{\partial x_i}\right)\qquad (\mathrm{i,j}=1,2,3)\ \text{in}\ \Omega \quad (1)$$

Mass conservation equation – the pseudo-compressibility form:

$$\frac{\partial p}{\partial t}+v_j\frac{\partial p}{\partial x_j}+\rho c_s^2\frac{\partial v_j}{\partial x_j}=0 \qquad (\mathrm{j}=1,2,3) \qquad \text{in}\ \Omega \qquad (2)$$

Energy conservation equation:

$$\frac{\partial T}{\partial t}+v_j\frac{\partial T}{\partial x_j}=\frac{1}{\rho c_v}\left(k\frac{\partial^2 T}{\partial x_j^2}+\rho S_T\right) \qquad (\mathrm{j}=1,2,3) \qquad \text{in}\ \Omega \qquad (3)$$

Pollutant transport equation:

$$\frac{\partial C}{\partial t}+v_j\frac{\partial C}{\partial x_j}=D\frac{\partial^2 C}{\partial x_j^2}+S_P \qquad (\mathrm{j}=1,2,3) \qquad \text{in}\ \Omega \qquad (4)$$

where v_i and S_i are components of the vectors of flow velocity and body force, respectively, which are given according to the direction of the Cartesian axes x_i, p is the thermodynamic pressure, T is the temperature, C is the pollutant concentration and δ_ij denotes the components of the Kroenecker's delta ($\delta_\mathrm{ij}=1$ for $i=j$; $\delta_\mathrm{ij}=0$ for $i\neq j$). The source terms for temperature and pollutant are denoted by S_T and S_P, respectively. The fluid properties are given by the fluid specific mass ρ, the kinematic viscosity ν, the bulk viscosity λ, the constant of isotropic thermal conductivity k, the constant of isotropic pollutant diffusion D, the specific heat at constant volume c_v and the sound speed in the flow field c_s. The governing equations are valid for a spatial domain Ω and a time interval $[t_0, t]$, where t_0 is the initial time, when initial conditions for the flow variables must be defined. In order to solve the system of governing equations, essential and natural boundary conditions for the flow variables must be also imposed over the spatial domain where the problem takes place.

Incompressible flows under thermal effects are generally analyzed using the Boussinesq's approximation, where density variations are considered in terms of body forces. By including effects of concentration, a general buoyancy force may be described as follows:

$$S_i=-\rho g_i\left[\beta(T-T_0)+\beta_C(C-C_0)\right] \qquad (5)$$

where β is the coefficient of volumetric expansion due to thermal effects, β_C is the coefficient of volumetric expansion due to concentration variation, g_i are the components of the vector of gravity acceleration **g**, which are given according to the direction of the Cartesian axes x_i, and

T_0 and C_0 are reference values for temperature and concentration, which are usually associated with undisturbed regions of the flow field. In the present work, the influence of concentration variations over the fluctuating gravitational forces (Eq. 5) is disregarded.

2.2 Turbulence modeling – LES

The main advantage of LES over turbulence models based on the RANS equations is related to the range of turbulence scales modeled. While RANS schemes try to model the full range of the energy spectrum and, consequently, all the turbulence scales, LES models are only concerned with scales below the size of a specified spatial filter, which is usually associated with the size of the finite elements for algorithms based on the FEM, whereas the turbulence scales above the filter size are solved directly. The basic step in the LES approach is the spatial filtering procedure performed over the flow variables, which are decomposed into components referring to large and sub-grid scales. Considering a general flow variable denoted by ϕ, the filtering operation can be mathematically described as the convolution of ϕ with a kernel G representing the filter function, that is:

$$\overline{\phi}\left(x_i,t\right)=\int_{\Omega}\phi\left(r_i,t\right)G\left(x_i-r_i,t\right)dr_i \tag{6}$$

where $\overline{\phi}$ is the large scale component of ϕ, such that $\phi=\overline{\phi}+\phi'$, where ϕ' is the SGS component of ϕ. The spatial field where the filtering operation takes place is indicated by Ω. For a box filter, the kernel function is defined by:

$$G\left(x_i-r_i,t\right)=\begin{cases}\displaystyle\prod_{i=1}^{n}\frac{1}{\overline{\Delta}_i} & \text{if } \left|x_i-r_i\right|\le\dfrac{\overline{\Delta}_i}{2}\\ 0 & \text{if } \left|x_i-r_i\right|>\dfrac{\overline{\Delta}_i}{2}\end{cases}\qquad (\mathrm{i}=1,\mathrm{n}) \tag{7}$$

where $\overline{\Delta}_i$ is the filter width in the i-th Cartesian direction and n is the number of dimensions of the filter operator.

By applying the filtering procedure (Eq. 6) over the flow governing equations (Eqs. 1-4), the advective terms lead to the SGS terms. The term involving SGS interactions in the momentum equations is referred to as SGS Reynolds stress tensor, which is usually defined as:

$$\sigma_{ij}^{SGS}=\rho\overline{v_i'v_j'} \tag{8}$$

In order to close the mathematical problem, the deviatoric part of the SGS Reynolds stress tensor is approximated using the Boussinesq eddy viscosity model as follows:

$$\tau_{ij}^{SGS}=\sigma_{ij}^{SGS}-\frac{1}{3}\sigma_{kk}^{SGS}\delta_{ij}=\sigma_{ij}^{SGS}-\frac{2}{3}\overline{E}_k\delta_{ij}\qquad\Rightarrow\qquad\tau_{ij}^{SGS}=-2\nu_t\overline{S}_{ij} \tag{9}$$

where $\overline{E}_k$ is the SGS turbulent kinetic energy, ν_t is the kinematic eddy viscosity and $\overline{S}_{ij}$ are the components of the strain rate tensor defined in terms of the large scale velocity field. The SGS terms in the heat and pollutant transport equations denote SGS turbulent fluxes of heat and pollutant, respectively, which may be written as:

$$-c_v\overline{v_j'T'}=k_t\frac{\partial\overline{T}}{\partial x_j}=\frac{\nu_t}{\mathrm{Pr}_t}\frac{\partial\overline{T}}{\partial x_j} \tag{10}$$

$$-\overline{v_j' C'} = D_t \frac{\partial \overline{C}}{\partial x_j} = \frac{\nu_t}{\mathrm{Sc}_t} \frac{\partial \overline{C}}{\partial x_j} \tag{11}$$

where k_t and D_t are the turbulent diffusivity coefficients for the heat and pollutant transport equations. These SGS terms are obtained using the eddy diffusivity assumption, where the turbulent Prandlt number $\mathrm{Pr_t}$ and the turbulent Schmidt number $\mathrm{Sc_t}$ are utilized.

The final form of the filtered governing equations, considering the eddy viscosity approach for the SGS terms, may be presented as follows:

$$\frac{\partial \overline{v}_i}{\partial t} + \overline{v}_j \frac{\partial \overline{v}_i}{\partial x_j} = -\frac{1}{\rho}\frac{\partial \overline{p}}{\partial x_i} + \frac{\partial}{\partial x_j}\left[2\left(\nu + \nu_t\right)\overline{S}_{ij} + \frac{\lambda}{\rho}\frac{\partial \overline{v}_k}{\partial x_k}\right] + \frac{1}{\rho}\overline{S}_i \qquad (\mathrm{i,j,k} = 1,2,3) \qquad \text{in } \Omega \tag{12}$$

$$\frac{\partial \overline{p}}{\partial t} + \overline{v}_j \frac{\partial \overline{p}}{\partial x_j} + \rho c_s^2 \frac{\partial \overline{v}_j}{\partial x_j} = 0 \qquad (\mathrm{j} = 1,2,3) \qquad \text{in } \Omega \tag{13}$$

$$\frac{\partial \overline{T}}{\partial t} + \overline{v}_j \frac{\partial \overline{T}}{\partial x_j} = \frac{\partial}{\partial x_j}\left[\left(\frac{k}{\rho c_v} + \frac{\nu_t}{\mathrm{Pr}_t}\right)\frac{\partial \overline{T}}{\partial x_j}\right] + \frac{1}{c_v}\overline{S}_T \qquad (\mathrm{j} = 1,2,3) \qquad \text{in } \Omega \tag{14}$$

$$\frac{\partial \overline{C}}{\partial t} + \overline{v}_j \frac{\partial \overline{C}}{\partial x_j} = \frac{\partial}{\partial x_j}\left[\left(D + \frac{\nu_t}{\mathrm{Sc}_t}\right)\frac{\partial \overline{C}}{\partial x_j}\right] + \overline{S}_P \qquad (\mathrm{j} = 1,2,3) \qquad \text{in } \Omega \tag{15}$$

Smagorinsky (1963) proposed to relate the eddy viscosity to the large scale flow field and the size of the numerical grid by using the following expression:

$$\nu_t = \left(C_S \overline{\Delta}\right)^2 \left|\overline{\mathbf{S}}\right| \tag{16}$$

where $\overline{\Delta}$ is the characteristic filter width, which may be locally obtained from the element volume for FEM formulations ($\overline{\Delta} = \sqrt[3]{\overline{\Delta}_1 \cdot \overline{\Delta}_2 \cdot \overline{\Delta}_3}$), $\left|\overline{\mathbf{S}}\right|$ is the modulus of the strain rate tensor and C_S is an empiric constant known as Smagorinsk's constant, with values usually ranging from 0.1 to 0.25. However, it is observed that C_S is not a universal constant, but it is flow dependent. In order to eliminate this shortcoming, the eddy viscosity ν_t can be also obtained employing the dynamic SGS model developed by Germano et al. (1991) and Lilly (1992), which may be expressed as:

$$\nu_t = C\left(\vec{x}, t\right)\overline{\Delta}^2 \left|\overline{\mathbf{S}}\right| \tag{17}$$

where $C\left(\vec{x}, t\right)$ is the dynamic coefficient, with $\vec{x}$ and t indicating space and time dependencies. The dynamic coefficient is updated along the time integration process taking into account instantaneous conditions of the flow field, that is:

$$C\left(\vec{x}, t\right) = -\frac{1}{2}\frac{L_{ij} M_{ij}}{M_{ij} M_{ij}} \tag{18}$$

where:

$$L_{ij} = \left\langle \overline{v}_i \overline{v}_j \right\rangle - \left\langle \overline{v}_i \right\rangle \left\langle \overline{v}_j \right\rangle \tag{19}$$

and:

$$M_{ij} = \left\langle \overline{\Delta} \right\rangle^2 \left| \left\langle \overline{S} \right\rangle \right| \left\langle \overline{S}_{ij} \right\rangle - \left\langle \overline{\Delta}^2 \left| \overline{S} \right| \overline{S}_{ij} \right\rangle \tag{20}$$

Nevertheless, the solution of Eq. (18) requires two filtering procedures on the flow governing equations: the first filtering is associated with the use of the LES formulation, where the spatial filter $\overline{\Delta}$ is applied in order to define the large scale variables $\overline{\phi}$; the second filtering is referred to another filter called test filter $\left\langle \overline{\Delta} \right\rangle$, which must be larger than the width of the first spatial filter $\overline{\Delta}$. Additional information on the evaluation of the filtered variables related to the second spatial filter is found in Braun and Awruch (2009b).

2.3 Numerical model

The numerical algorithm for the flow analysis is formulated considering the two-step Taylor-Galerkin model (see Braun and Awruch, 2009a). In this method, the governing equations are temporally discretized using second-order Taylor series expansions and the Bubnov-Galerkin method is applied to the system of equations obtained from the time discretization procedure. Finite element approximations for the spatial and variable fields are performed here considering the eight-node hexahedral element formulation. The element matrices are evaluated employing the one-point quadrature technique, where the origin of the parametric space is chosen as the only quadrature point. This integration technique leads to analytical evaluation of the matrix components, which is exact for elements with parallel faces. Good results can be also obtained for slightly distorted elements, but they are not strictly exact. Nevertheless, spurious modes (hourglass modes) must be suppressed using some hourglass control scheme in order to obtain reliable results. An algorithm describing the numerical scheme utilized here to solve the governing equations may be found in Table 1, where the overbars representing the large scale variables are omitted for the sake of simplicity.

---

1) *The first step*: calculate the flow variables at the intermediate point of the time increment Δt:

$$v_i^{n+1/2} = v_i^n + \frac{\Delta t}{2}\left\{ -v_j \frac{\partial v_i}{\partial x_j} - \frac{1}{\rho}\frac{\partial p}{\partial x_j}\delta_{ij} + \frac{\partial}{\partial x_j}\left[(\nu + \nu_t)\left(\frac{\partial v_i}{\partial x_j} + \frac{\partial v_j}{\partial x_i} \right) + \frac{\lambda}{\rho}\frac{\partial v_k}{\partial x_k}\delta_{ij} \right] + \left(\frac{\Delta t}{4} v_j v_k \right)\frac{\partial^2 v_i}{\partial x_j x_k} + \frac{S_i}{\rho} \right\}^n$$

$$p^{n+1/2} = p^n + \frac{\Delta t}{2}\left\{ \left[-v_j \frac{\partial p}{\partial x_j} - \rho c^2 \frac{\partial v_j}{\partial x_j} \right] + \left(\frac{\Delta t}{4} v_i v_j \right)\frac{\partial^2 p}{\partial x_j \partial x_i} \right\}^n$$

$$T^{n+1/2} = T^n + \frac{\Delta t}{2}\left\{ -v_j \frac{\partial T}{\partial x_j} + \left(\frac{k}{\rho c_v} + \frac{\nu_t}{\mathrm{Pr}_t} \right)\frac{\partial^2 T}{\partial x_j^2} + \left(\frac{\Delta t}{4} v_i v_j \right)\frac{\partial^2 T}{\partial x_j \partial x_i} + \frac{1}{c_v} S_T \right\}^n$$

$$C^{n+1/2} = C^n + \frac{\Delta t}{2}\left\{ -v_j \frac{\partial C}{\partial x_j} + \left(D + \frac{\nu_t}{\mathrm{Sc}_t} \right)\frac{\partial^2 C}{\partial x_j^2} + \left(\frac{\Delta t}{4} v_i v_j \right)\frac{\partial^2 C}{\partial x_j \partial x_i} + S_C \right\}^n$$

2) Apply the boundary conditions on $v_i^{n+1/2}$, $p^{n+1/2}$, $T^{n+1/2}$ and $C^{n+1/2}$.

---

3) Calculate the pressure increment $\Delta p^{n+1/2} = p^{n+1/2} - p^n$.

4) Calculate the corrected velocity field with the updated pressure $\Delta p^{n+1/2}$:

$$v_i^{n+1/2} = v_i^{n+1/2} - \frac{1}{\rho}\frac{\Delta t^2}{8}\frac{\partial \Delta p^{n+1/2}}{\partial x_i}$$

5) Apply the boundary condition on $v_i^{n+1/2}$.

6) *The second step*: update the flow variables at the end of the time increment Δt:

$$v_i^{n+1} = v_i^n + \Delta v_i^{n+1/2}$$

$$p^{n+1} = p^n + \Delta p^{n+1/2}$$

$$T^{n+1} = T^n + \Delta T^{n+1/2}$$

$$C^{n+1} = C^n + \Delta C^{n+1/2}$$

where:

$$\Delta v_i^{n+1/2} = \Delta t\left\{-v_j\frac{\partial v_i}{\partial x_j} - \frac{1}{\rho}\frac{\partial p}{\partial x_j}\delta_{ij} + \frac{\partial}{\partial x_j}\left[\left(\nu+\nu_t\right)\left(\frac{\partial v_i}{\partial x_j}+\frac{\partial v_j}{\partial x_i}\right)+\frac{\lambda}{\rho}\frac{\partial v_k}{\partial x_k}\delta_{ij}\right]+\frac{S_i}{\rho}\right\}^{n+1/2}$$

$$\Delta p^{n+1/2} = \Delta t\left\{-v_j\frac{\partial p}{\partial x_j} - \rho c^2\left(\frac{\partial v_j}{\partial x_j}\right)\right\}^{n+1/2}$$

$$\Delta T^{n+1/2} = \Delta t\left\{-v_j\frac{\partial T}{\partial x_j} + \left(\frac{k}{\rho c_v}+\frac{\nu_t}{\mathrm{Pr}_t}\right)\frac{\partial^2 T}{\partial x_j^2} + \frac{1}{c_v}S_T\right\}^{n+1/2}$$

$$\Delta C^{n+1/2} = \Delta t\left\{-v_j\frac{\partial C}{\partial x_j} + \left(D+\frac{\nu_t}{\mathrm{Sc}_t}\right)\frac{\partial^2 C}{\partial x_j^2} + \frac{1}{c_p}S_C\right\}^{n+1/2}$$

7) Apply the boundary conditions on v_i^{n+1}, p^{n+1}, T^{n+1} and C^{n+1}.

8) Return to 1) for the next time step Δt.

Table 1. Numerical algorithm for the flow analysis.

The time interval used in the time discretization scheme is restricted by the Courant condition in order to maintain numerical stability, since the time integration is carried out explicitly. A critical value can be calculated at element level by using the following expression:

$$\Delta t_{\mathrm{E}} = \alpha\frac{\Delta x_{\mathrm{E}}}{\mathrm{V}_{\mathrm{E}} + c_s} \qquad \mathrm{E}\in\left[1, NE\right] \tag{21}$$

where Δx_E is the characteristic width of element E, V_E is a characteristic flow speed of element E, c_s is the sound speed in the flow field, α is a safety constant, which is generally

less than unity, and *NE* is the number of elements in the finite element mesh. Although independent time steps can be adopted, the time step employed in the numerical applications carried out in this work is obtained from the smaller time step calculated with Eq. (21).

3 NUMERICAL APPLICATIONS

3.1 Lid-driven cavity analysis

In the present application numerical analyses of two-dimensional flows in a lid-driven cavity are performed in order to demonstrate the accuracy of the formulation proposed in this work when it is applied to the cavity flow problem, which characterizes the flow conditions found in the urban street canyon environment. It is important to notice that the numerical model employed in this paper was also validated previously using applications on building aerodynamics under isothermal flow conditions (see Braun and Awruch, 2009a). For the present investigation, isothermal and non-isothermal analyses are considered, where the flow is characterized by the classical dimensionless numbers of fluid mechanics. Geometric characteristics and boundary conditions utilized here to reproduce the cavity flow are shown in Fig. 1, where one can notice that a vertical gradient is imposed on the temperature field if non-isothermal conditions are taken into account. In addition, the finite element mesh employed in the present studies is also presented observing that 100x100x1 eight-node hexahedral elements are utilized with the most refined elements located along the cavity walls ($\Delta x_E = 0.0025$ m).

In Table 2, the flow properties adopted in the numerical analyses are presented according to the different investigations carried out here, where the time step was calculated using Eq. (21) with $\alpha = 0.44$, which leads to $\Delta t = 10^{-4}$ s. Notice that the Mach number may be interpreted as a penalty parameter for the mass conservation equation adopted in the present model. LES with the Smagorinsky's SGS model were utilized for turbulent flows considering $C_S = 0.15$.

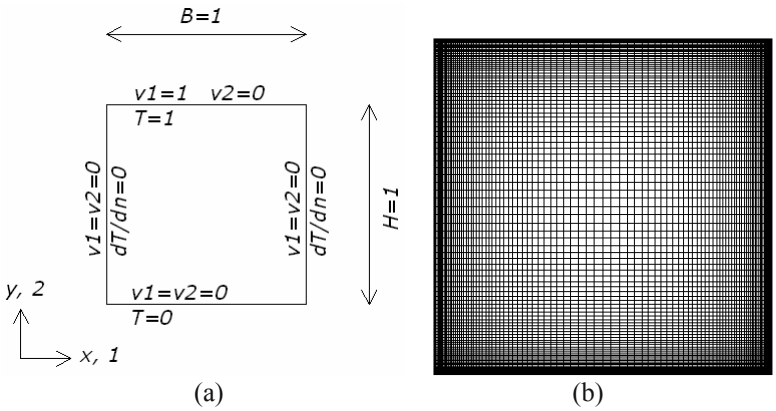

Figure 1. Lid-driven cavity analysis: (a) geometrical domain and boundary conditions; (b) finite element mesh.

Flow properties	Flow conditions				
	Isothermal		Non-isothermal		
	Flow 1	Flow 2	Flow 3	Flow 4	Flow 5
Reynolds number (Re)	10^3	10^4	10^3	10^3	10^4
Prandtl number (Pr)	-	-	0.71	0.71	0.71
Turbulent Prandtl number (Pr_t)	-	-	0.71	0.71	0.71
Mach number (Ma)	0.1	0.1	0.1	0.1	0.1
Grashof number (Gr)	-	-	10^2	10^6	10^7

Table 2. Lid-driven cavity analysis: flow properties.

Figure 2 shows velocity profiles obtained with the present model along the horizontal and vertical centerlines of the cavity for all the flow conditions investigated, which are compared with numerical predictions obtained by Ghia et al. (1982) and Agrawal et al. (2001). A very good agreement can be observed.

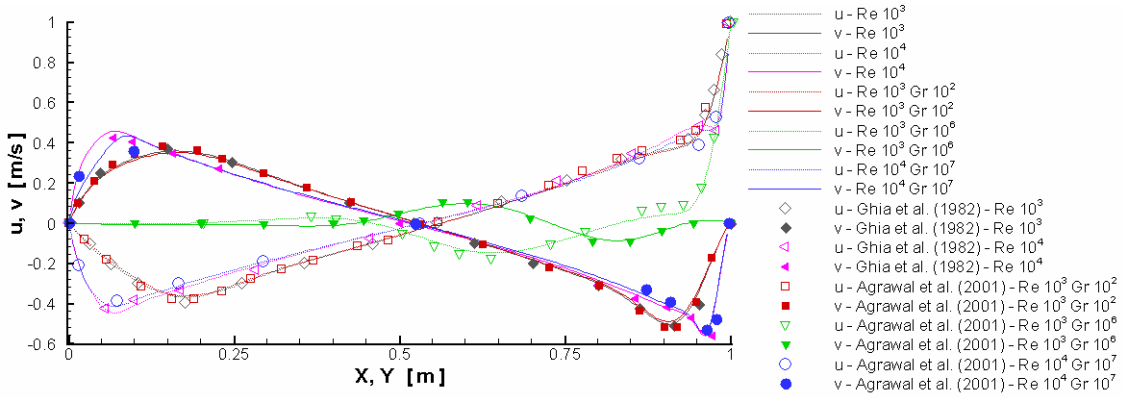

Figure 2. Lid-driven cavity analysis: velocity profiles along the centerlines of the cavity.

Streamlines and temperature contour lines obtained in the present investigations are shown in Fig. 3. One can observe that the isothermal cases analyzed here reproduced very well the circulation pattern presented by Ghia et al. (1982), where a main circulation is found in the central region of the cavity and secondary vortices are developed at the corners of the ground level. Moreover, a third vortex is obtained at the left corner of the top level when the flow becomes turbulent (Re = 10^4). For non-isothermal conditions, the flow pattern is similar to that obtained by Agrawal et al. (2001). It is observed that the streamlines obtained for Gr = 10^2 are approximately the same as that presented under isothermal conditions. In addition, strong temperature gradients are concentrated near the bottom of the cavity and a weak gradient is found in the central area. On the other hand, when a higher Grashof number is considered, i.e. Gr = 10^6, the flow circulation is restricted to a region close to the top of the cavity and the remaining regions present a nearly stagnant flow. The heat transfer over the cavity is predominantly conductive and only a small portion near the top is influenced by the action of advection induced by the lid motion. Under turbulent flow conditions (Re = 10^4), the circulation is extended again to the whole cavity and the temperature field is highly influenced by advection.

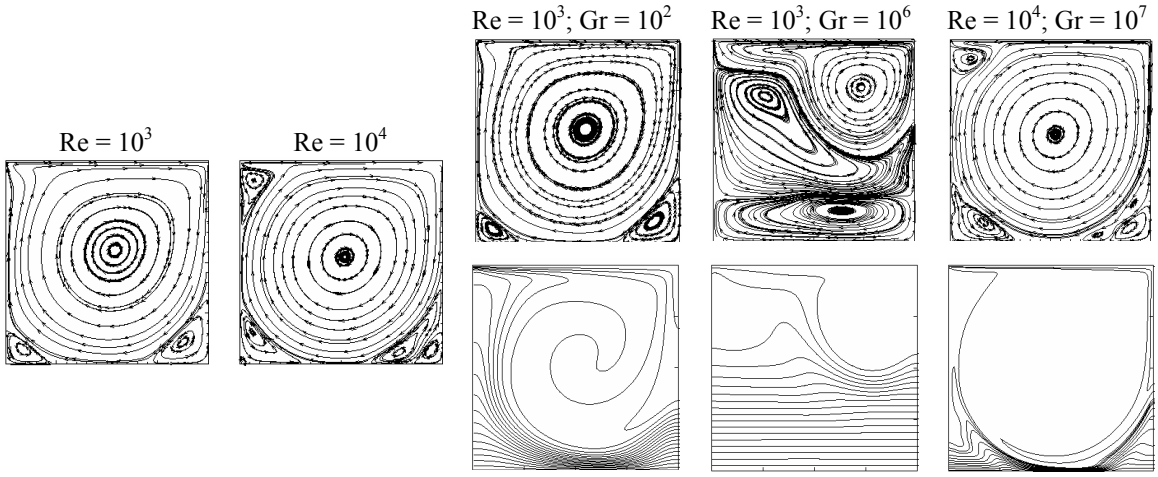

Figure 3. Lid-driven cavity analysis: streamlines and isotherms according to different flow conditions.

3.2 Pollutant dispersion in a two-dimensional street canyon

This application is dedicated to evaluate the pollutant dispersion in a 2-D urban street canyon with unitary aspect ratio (H/W = 1), considering isothermal conditions. The computational domain and the boundary conditions adopted in the present study are show in Fig. 4. It is important to notice that no-slip boundary conditions are imposed on the street canyon surfaces. In the same figure, the finite element mesh employed is also presented. The spatial field is discretized using 8400 eight-node hexahedral elements. The smaller elements are found along the canyon walls, where $\Delta x_E = 0.001$ m. A pollutant is emitted from a point source located at the bottom of the canyon model (see Fig. 4 (a)) and the emission rate is defined as $S_P = 2.89 \times 10^{-5}$ m^3/s.

The flow properties adopted in the numerical model are characterized by the following dimensionless numbers: $Re = 1.2 \times 10^4$, Ma = 0.1and $Sc = Sc_t = 0.72$. The flow variables are started with zero initial conditions and the time step is chosen taking into account Eq. (21) with $\alpha = 0.27$, which leads to a time step of $\Delta t = 10^{-5}$ s. Turbulence is simulated using LES with the dynamic SGS model. The Reynolds number is evaluated considering the height (H) of the street canyon model and the undisturbed flow velocity at $z = 0.65$ m, i.e. $V_\infty = 2.0$ m/s (see Fig. 4 (a)). The numerical analyses were performed up to $t = 110$ s, where a time average flow field with statistically constant characteristics is obtained. The time average fields were calculated taking into account the last 10 s of the present analyses.

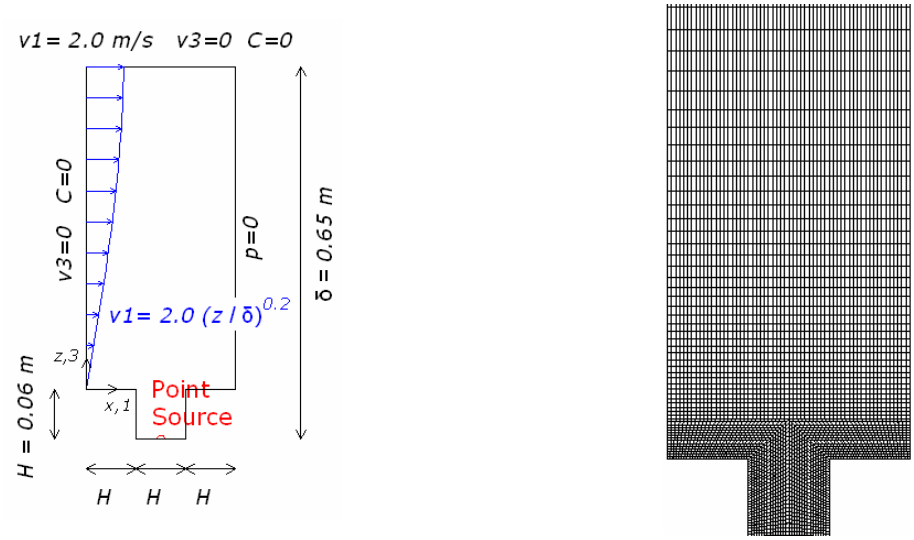

(a) (b)

Figure 4. Two-dimensional street canyon: (a) geometrical domain and boundary conditions; (b) finite element mesh.

Figure 5 shows results obtained with the numerical model proposed in this work, where time average fields referring to streamlines, pressure, flow velocity components and pollutant concentration are presented. One can notice that a main vortex is generated along with secondary vortices located at the corners of the canyon, and the pollutant concentration follows the flow observed in the main recirculation region, which carries the pollutant towards the roof level, where it is partially removed.

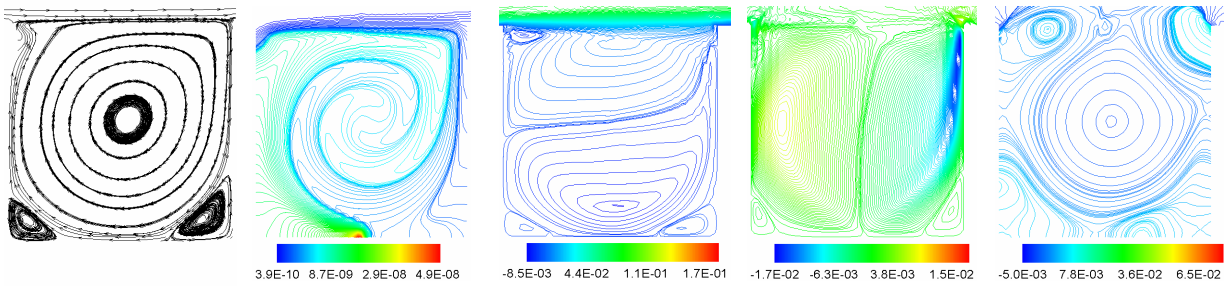

(a) (b) (c) (d) (e)

Figure 5. Two-dimensional street canyon: time average fields in the canyon – streamlines (a); pollutant concentration (b); flow velocity components v1 (c), and v3 (d) and pressure (e).

Profiles referring to the dimensionless pollutant concentration C* measured along vertical (a) and horizontal (b) lines of the canyon model are presented in Fig. 6. In this figure, results obtained with the numerical model proposed in the present work are shown and compared with results obtained experimentally by Meroney et al. (1996) [ref. 1] and Pavageau and Schatzmann (1999) [ref. 2] and numerically by Popiolek (2005) [ref. 3], considering the reference length utilized in the definition of the Reynolds number Re (H_{ref}) are equal to 1H and 3H. One can observe that a good agreement is obtained considering comparisons performed with respect to concentration distribution in the canyon cavity, especially when H_{ref} = 3H is adopted.

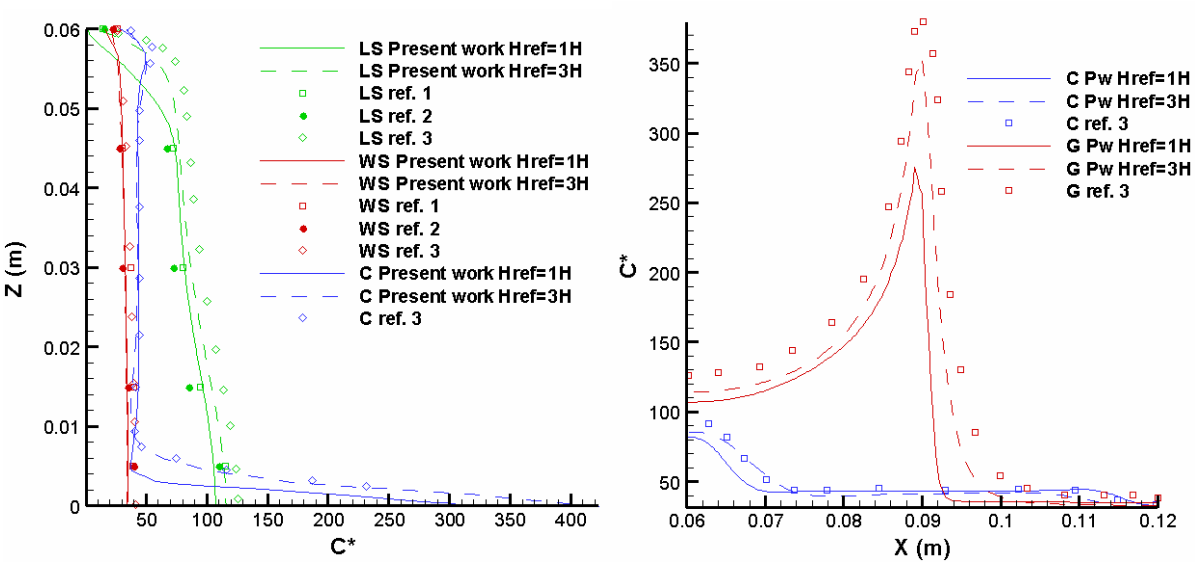

(a) (b)

Figure 6. Two-dimensional street canyon: dimensionless concentration C* distributions along vertical lines (a) - on the leeward side (LS), windward side (WS) and central line (C); and horizontal lines (b) – on the central line (C) and near ground level (G).

3.3 Pollutant dispersion in a three-dimensional street canyon

In this application, a three-dimensional street canyon was considered according to the studies performed by Salim et al. (2011). A schematic view of the computational domain utilized here and the mesh configuration in the region of the buildings are found in Fig. 7, where boundary conditions are also indicated. The finite element mesh is constituted by 1371500 eight-node hexahedral elements, with $\Delta x_E \approx 0.05$ m, which is related to the smaller elements located along the building and ground surfaces. The positions of the linear pollutant sources, which approximately reproduce emission conditions observed under intense traffic of motor vehicles, are also shown. In order to account for the traffic exhausts released on sidewise street intersections, the line sources exceed the street canyon length by approximately 10% on each side. The pollutant sources are characterized with an emission rate of $S_P = 0.01$ m^3/s.

The flow properties adopted in the numerical model are characterized by the following dimensionless numbers: Re = 3.76 x 10^4, Ma = 0.16 and Sc = Sc_t = 0.7. Turbulence is simulated considering LES and both, the classical Smagorisky's SGS model, where C_S = 0.12, and the dynamic SGS model. The flow variables are started with zero initial conditions, where the time step is chosen taking into account Eq. (21) with $\alpha = 0.51$, which leads to Δt = 7.5 x 10^{-4} s. The Reynolds number is obtained considering the building height and the flow velocity at the roof level (see Fig. 7 (a)). The numerical analysis was carried out up to t = 1500 s and time average fields were obtained over the last 200 s of the present simulation. The simulations presented here were performed using the OpenMP API's and an intel core i7 2600 quad core processor. A typical run time for the present application is approximately 3333.3 hours.

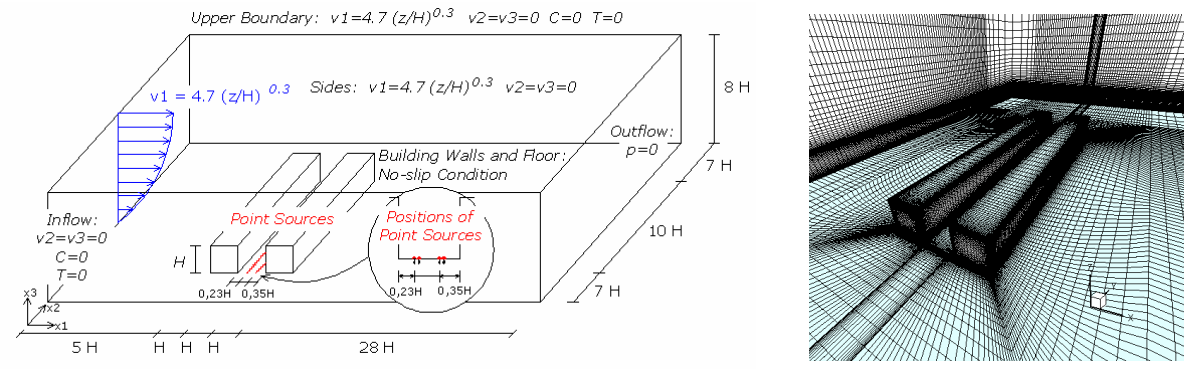

(a) (b)

Figure 7. Three-dimensional street canyon: (a) geometrical domain and boundary conditions; (b) finite element mesh.

Fig. 8 presents the time average streamlines and time average pollutant concentration fields for the plane x - z (y = 60 m), obtained when the classical Smagorisky's SGS model [CM] and the dynamic SGS model [DM] were used. When the classical model is adopted, one can notice that the streamlines passing through the first building detach and don't reattach along the top surface of this building. Streamlines originated from a clockwise recirculation zone formed over the last building move along the main flow in the opposite direction to the top of the first building, influencing the circulation pattern within the canyon. A main counterclockwise recirculation zone and two secondary clockwise vortices located at the corners of the canyon are formed in the canyon cavity. Behind the second building, a stationary secondary counterclockwise vortex is formed near the floor and a recirculation zone, which extends over a distance of 4H in the flow direction, is generated near the rear wall. On the other hand, when the dynamic model is employed, one can notice a small recirculation zone formed near the upstream roof edge of the first building. Furthermore, a clockwise recirculation is generated inside the canyon, which extends in the vertical direction beyond the height of the buildings. Two secondary counterclockwise vortices are generated in the bottom corners of the canyon. As previously observed, a stationary counterclockwise vortex is formed behind the second building and a recirculation zone, which extends over a distance of 3H in the flow direction, is generated near the rear wall, which streamlines do not communicate with the internal flow of the canyon. Analyzing Figs. 8 (c), one can notice that, for both turbulence models used, the secondary vortices, which are located inside the canyon, spread the pollutants in the region near the ground. According to the direction of the main recirculation developed inside the canyon, the pollutants are removed from the canyon. When the classical model is adopted, there is a counterclockwise main recirculation and pollutants tend to be removed through the windward wall (wall B). However, when the dynamic model is used, a clockwise main recirculation is observed and the pollutants tend to leave the canyon by the leeward wall (wall A).Through the flow established in the upper canyon region, the pollutants are carried by the main flow in the opposite direction to the top of the first building and then, they are carried downstream by the main flow.

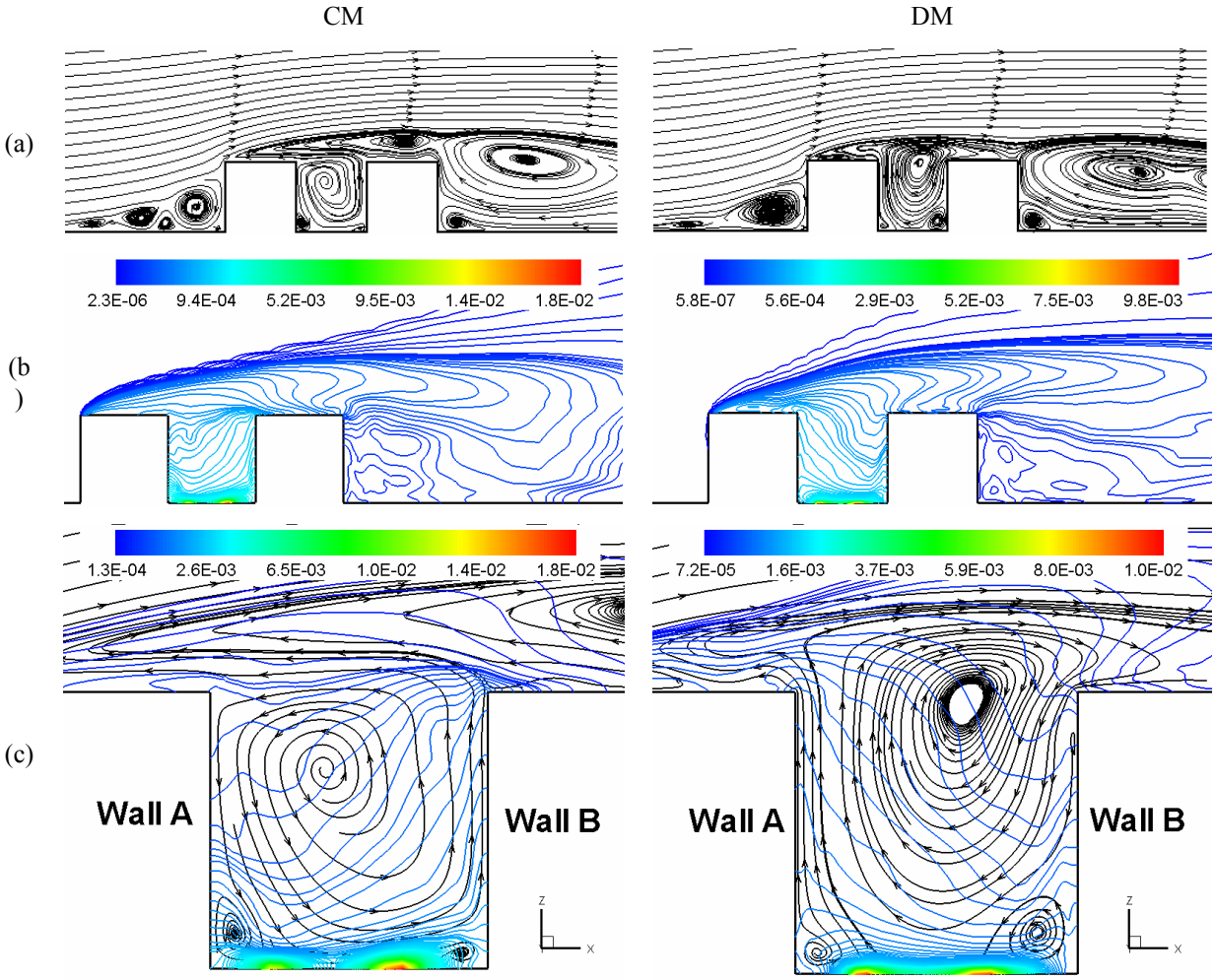

Figure 8. Three-dimensional street canyon: time average fields on plane y = 60 m - streamlines and pollutant concentration.

Time average streamlines obtained in the present analysis for the planes x - z (y = 60 m and y = 50 m) and plane x - y (z = 1 m and z = 2 m) are shown in Fig. 9, where flow phenomena such as horseshoe vortices can be observed. One can notice that this flow configuration presents two vortices, when the classical model is used, and only a larger vortex, when the dynamic model is used.

An overview of the pollutant dispersion around the buildings is presented in Fig. 10, taking into account horizontal planes corresponding to different levels of the computational domain. Pollutant concentration contours on the canyon leeward (wall A) and windward (wall B) walls are presented in Fig. 11. Observing these figures, one can notice that when the classical model is adopted, the counterclockwise main recirculation developed on the intermediate plane of the canyon (y = 60 m) (see Fig. 8 (c) for CM) makes the pollutant concentration levels on wall B higher than the pollutant concentration levels observed on wall A (see Figs. 10 and 11 for CM). On the other hand, when the dynamic model is used, there is a clockwise main recirculation in this plane (see Fig. 8 (c) for DM), which makes the pollutant concentration levels on wall A higher than the pollutant concentration levels observed on wall B (see Figs. 10 and 11 for DM). Looking also at Figs. 10 and 11, it is observed that the pollutants are concentrated in the central region of the canyon when both turbulence models are considered.

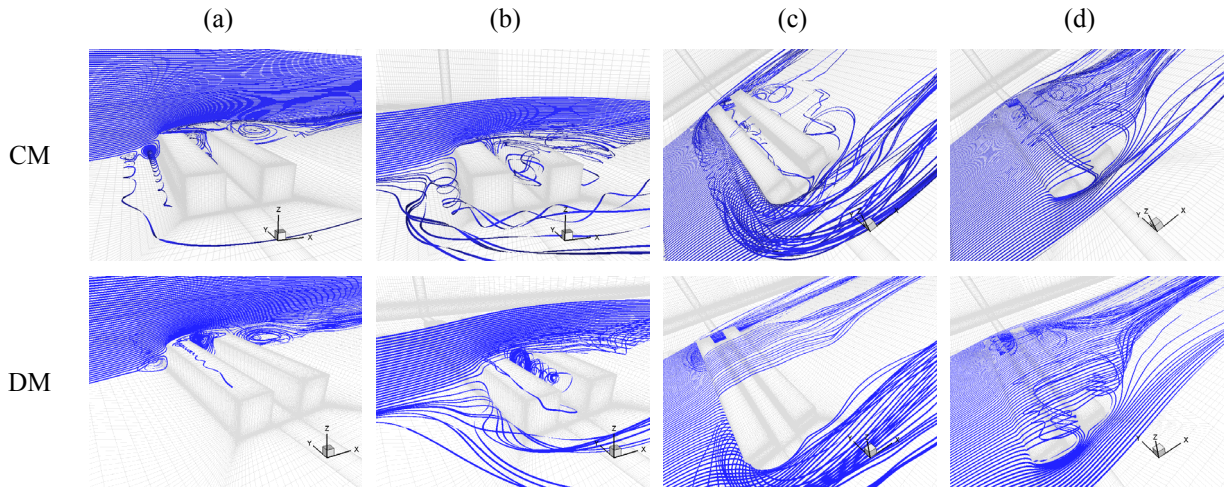

Figure 9. Three-dimensional street canyon: time average streamlines at y = 60 m (a); at y = 50 m (b); at z = 1 m (c) and at z = 2.0 m (d).

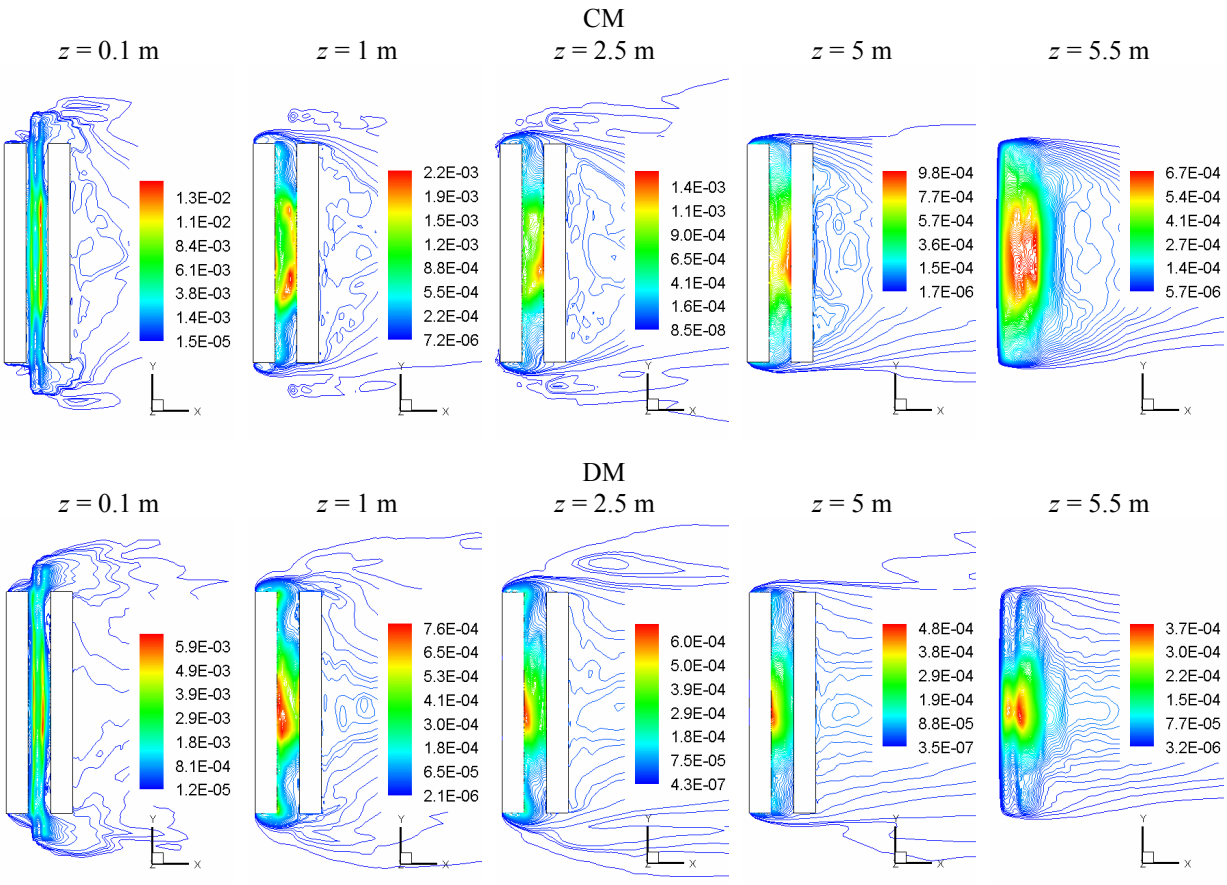

Figure 10. Three-dimensional street canyon: time average fields on plane x-y considering different heights: pollutant concentration.

Salim et al. (2011), using turbulent intensities in the incident wind flow, obtained experimentally and numerically higher pollutant concentration levels on wall A, if compared with the values found on wall B. Analyzing this behavior, the results obtained in the present

work with the dynamic SGS model would be most appropriated. Nevertheless, differences are observed when velocity and pollutant concentration fields obtained in the present work are compared with those from reference. It is important to notice that these different results depend on the flow pattern developed in the canyon, which extends beyond the height of the canyons in the present work.

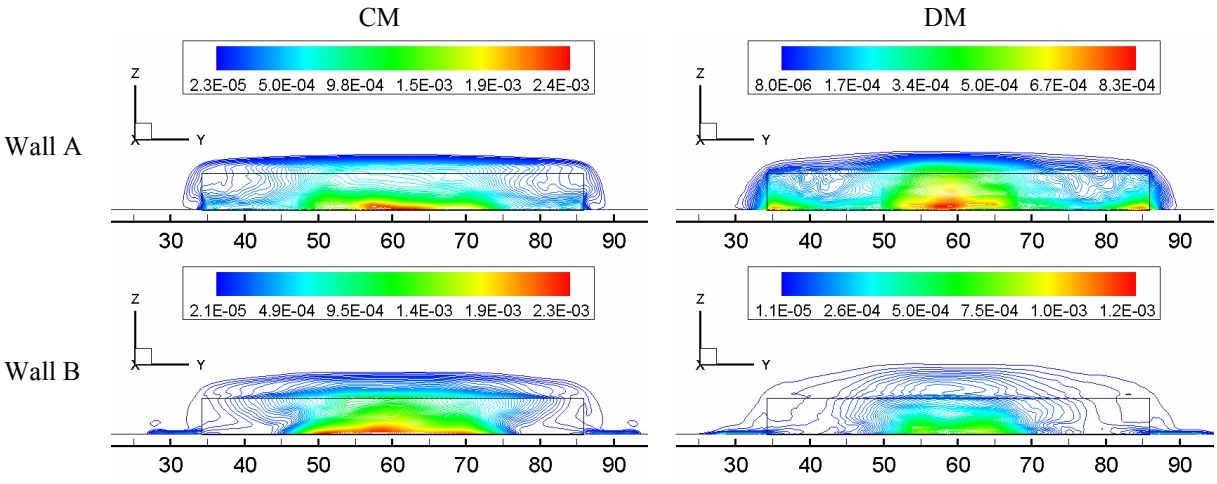

Figure 11. Three-dimensional street canyon: time average fields on plane y - z for pollutant concentration on wall A (x = 30 m) and wall B (x = 35 m).

4 CONCLUSIONS

A numerical model to investigate urban street canyon flows was presented in this work, where a finite element formulation for eight-node hexahedral elements with one-point quadrature was considered. The formulation proposed by Braun and Awruch (2009a) for investigations on building aerodynamics was extended here to deal with problems of heat and mass transport in the urban microscale. In the present model, the governing equations for incompressible flows with heat and mass transfer were formulated taking into account the pseudo-compressibility hypothesis for explicit evaluation of the pressure field and LES for turbulence simulation. The present model was validated using the cavity flow problem under isothermal and non-isothermal conditions, which characterize the flow conditions usually found in urban street canyons. A two-dimensional street canyon configuration under isothermal conditions was investigated and results demonstrated good agreement with predictions reported by other authors. Finally, a three-dimensional problem was proposed and the flow and pollutant dispersion surrounding the street canyon was reproduced, where the sub-grid scales are modeled using both, the classical Smagorinsky`s model and the dynamic model. The flow characteristics observed in the street canyons were analyzed and significant differences were observed when both SGS models are considered. These differences between results may be related to the finite element mesh utilized here, which presented poor refinement in the canyon region, where 35 x 41 elements were employed. Previous studies carried out in a two-dimensional street-canyon model, where the canyon region was discretized using 120 x 120 elements, presented similar results when these two SGS models were used (see Madalozzo et. al., 2012). The results obtained using the dynamic SGS model are the most appropriate if compared with the results reported by Salim et al. (2011), since the pollutant distribution on wall A and B are similar. However, differences in the velocity and pollutant concentration fields are observed. Thus, further studies considering finer meshes and

turbulent intensities in the incident wind flow should be performed in order to verify the results presented here. An important aspect related to the numerical model is the safety factor α utilized in the stability condition (Eq. 21), which was significantly reduced in this work when compared to the values usually employed in Braun and Awruch, 2009a, where only isothermal flows without source terms were investigated. Moreover, for future works, a model to consider chemical reactions of air pollutants should be implemented in order to improve the numerical description of the physical phenomena observed in street canyon flows.

REFERENCES

Agrawal, L., Mandal, J. C., and Marathe, A. G., 2001. Computations of laminar and turbulent mixed convection in a driven cavity using pseudo-compressibility approach. Computers & Fluids, vol. 30, pp. 607-620.

Ahmad, K., Khare, M., Chaudhry, K.K., 2005. Wind tunnel simulation studies on dispersion at urban street canyons and intersections: a review. Journal of Wind Engineering and Industrial Aerodynamics, vol. 93, pp. 697-717.

Baik, J.J., Kang, Y.S., Kim, J.J., 2007. Modeling reactive pollutant dispersion in an urban street canyon. Atmospheric Environment, vol. 41, pp. 934-949.

Baik, J.-J., Kim, J.-J., 1999. A numerical study of flow and pollutant dispersion characteristics in urban street canyons. Journal of Applied Meteorology, vol. 38, pp. 1576-1589.

Baik, J.-J., Kim, J.-J., Fernando, H.J.S., 2003. A CFD model for simulating urban flow and dispersion. Journal of Applied Meteorology, vol. 42, pp. 1636-1648.

Baker, J., Walker, H.L., Cai, X., 2004. A study of the dispersion and transport of reactive pollutants in and above street canyons e a large eddy simulation. Atmospheric Environment, vol. 38, pp. 6883-6892.

Berkowicz, R., Hertel, O., Larsen, S.E., Sorensen, N.N., Nielsen, M., 1997. Modelling traffic pollution in streets. Technical Report: NERI, Roskilde, Denmark.

Blocken, B., 2011. Computational Wind engineering: theory and applications. In: Environmental Wind Engineering and Desing of Wind Energt Structures, C.C. Baniotopoulos et al. (eds.), Udine-ITA, vol. 51, pp. 55-93.

Braun, A.L., Awruch, A.M., 2008. Finite element simulation of the wind action over bridge sectional models: application to the Guamá River Bridge (Pará State, Brazil). Finite Elements in Analysis and Design, vol. 44, pp. 105-122.

Braun, A.L., Awruch, A.M., 2009a. Aerodynamic and aeroelastic analyses on the CAARC standard tall building model using numerical simulation. Computers and Structures, vol. 87, pp. 564-581.

Braun, A.L., Awruch, A.M., 2009b. An energy-conserving partitioned model for fluid-structure interaction problems using hexahedral finite elements with one-point quadrature. International Journal for Numerical Methods in Engineering, vol. 79, pp. 505-549.

Ca, V.T., Asaeda, T., Ito, M., Armfield, S., 1995. Characteristics of wind field in a street canyon. Journal of Wind Engineering and Industrial Aerodynamics, vol. 57, pp. 63-80.

Carpenter, L.J., Clemitshaw, K.C., Burgess, R.A., Penkett, S.A., Capes, J.N., McFadyen, 1998. Investigation and evaluation of the NOx/O3 photochemical steady state. Atmospheric Environment, vol. 32, pp. 3353-3365.

Carter, W.P.L., 1994. Development of ozone reactivity scales for volatile organic compounds. Journal of the Air and Waste Management Association, vol. 44, pp. 881-899.

Chabni, A., Le Que´re´, P., Tenaud, C., Laatar, H., 1998. Modelling of pollutant dispersion in urban street canyons by means of a large-eddy simulation. International Journal of Vehicle Design, vol. 20, pp. 88-95.

Chan, A.T., AU, W.T.W., So, E.S.P., 2003. Strategic guidelines for street canyon geometry to achieve sustainable street air quality. Part II: multiple canopies and canyons. Atmospheric Environment, vol. 37, pp. 2761-2772.

Chan, T.L., Dong, G., Leung, C.W., Cheung, C.S., Hung, W.T., 2002. Validation of a two-dimensional pollutant dispersion model in an isolated street canyon. Atmospheric

Environment, vol. 36, pp. 861-872.
Cheng, W.C., Liu, C-H., 2011. Large-eddy simulation of turbulent transports in urban street canyons in different thermal stabilities. Journal of Wind Engineering and Industrial Aerodyanmics, vol. 99, pp. 434-442.
Cui, Z., Cai, X.M., Baker, C.J., 2004. Large eddy simulation of turbulent flow in a street canyon. Quarterly Journal of the Royal Meteorological Society, vol. 599, pp. 1373-1394.
Dodge, M.C., 2000. Chemical oxidant mechanisms for air quality modeling critical review. Atmospheric Environment, vol. 34, pp. 2103-2130.
Garmory, A., Kim, I.S., Britter, R.E., Mastorakos, E., 2009. Simulations of the dispersion of reactive pollutants in a street canyon, considering different chemical mechanisms and micromixing. Atmospheric Environment, vol. 43, pp. 4670-4680.
Germano, M., Piomelli, U., Moin, P., Cabot, W.H., 1991. A dynamic subgrid-scale eddy viscosity model. Physics of Fluids, vol. A3, pp. 1760-1765.
Ghia, U., Ghia, K.N., Shin, C.T., 1982. High-Re Solutions for Incompressible Flow Using the Navier-Stokes Equations and a Multigrid Method. Journal of Computational Physics, vol. 48, pp. 387-411.
Gidhagen, L., Johansson, C., Langner, J., Foltescu, V.L., 2005. Urban scale modeling of particle number concentration in Stockholm. Atmospheric Environment, vol. 39, pp. 1711-1725.
Gosseau, P., Blocken, B., Stathopoulos, T., van Heijst, G., 2010. CFD simulation of pollutant dispersion around buildings: comparison between RANS k-ε and LES approaches. In: Proceedings of The Fifth International Symposium on Computational Wind Engineering (CWE 2010), Chapel Hill, USA.
Grawe, D., Cai, X.M., Harrison, R.M., 2007. Large eddy simulation of shading effects on NO2 and O3 concentrations within an idealised street canyon. Atmospheric Environment, vol. 41, pp. 7304-7314.
Hajra, B., 2011. Recent studies in CFD modelling of pollutant dispersion in street canyons. Building Simulation, online, pp. 1-12.
Iizuka, S., Kondo, H., 2004. Performance of various sub-grid scale models in large-eddy simulations of turbulent flow over complex terrain. Atmospheric Environment, vol. 38, pp. 7083-7091.
Jeong, S. J., Andrews, M.J., 2002: Application of the k-ε turbulence model to the high Reynolds number skimming flow field of an urban street canyon. Atmospheric Enviroment, vol. 36, pp. 1137-1145.
Kang, Y.S., Baik, J.J., Kim, J.J., 2008. Further studies of flow and reactive pollutant dispersion in a street canyon with bottom heating. Atmospheric Environment, vol. 42, pp. 4964-4975.
Kastner-Klein, P., Plate, E.J., 1999. Wind-tunnel study of concentration fields in street canyons. Atmospheric Environment, vol. 33, pp. 3973-3979.
Kikumoto, H., Ooka, R., 2011. A study on the air pollutants dispersion with bimolecular reactions in urban street canyons using LES. In: Proceedings of the 13th International Conference on Wind Engineering (ICWE13), Amsterdam, Netherlands.
Kim, J-J and Baik, J-J., 1999. A numerical study of thermal effects on flow and pollutant dispersion in urban street canyons. Journal of Applied Meteorology, vol. 38, pp. 1249-1261.
Kim, J-J., Baik, J-J., 2001. Urban street-canyon flows with bottom heating. Atmospheric Environment, vol. 35, pp. 3395-3404.
Kumar, P., Fennell, P., Britter, R., 2008a. Effect of wind direction and speed on the dispersion of nucleation and accumulation mode particles in an urban street canyon. Science of the Total Environment, vol. 402, pp. 82-94.
Kumar, P., Fennell, P., Langley, D., Britter, R., 2008b. Pseudo-simultaneous measurements for the vertical variation of coarse, fine and ultrafine particles in an urban street canyon. Atmospheric Environment, vol. 42, pp. 4304-4319.
Kwak, K-H., Baik, J-J., 2012. A CFD modeling study of the impacts of NO_X and VOC emissions on reactive pollutant dispersion in and above a street canyon. Atmospheric Environment, vol. 46, pp. 71-80.

Lee, I.Y., Park, H.M., 1994. Parameterization of the pollutant transport and dispersion in urban street canyons. Atmospheric Environment, vol. 28, pp. 2343-2349.
Leriche, E., Gavrilakis, S., 2000: Direct numerical simulation of the flow in a lid-driven cubical cavity. Physics of Fluids, vol. A12, pp. 1363-1376.
Li, X.X., Koh, T.Y., Britter, R., Liu, C.H., Norford, L.K., Entekhabi, D., Leung, D.Y.C., 2009. Large-eddy simulation of flow field and pollutant dispersion in urban street canyons under unstable stratification. In: Proceeding of the 7th International Conference on Urban Climate (ICUC-7), Yokohama, Japan.
Li, X.-X., Liu, C.-H., Leung, D.Y.C., 2008. Large-eddy simulation of flow and pollutant dispersion in high-aspect-ratio urban street canyons with wall model. Boundary-Layer Meteorology, vol. 129, pp. 249-268.
Li, X.X., Liu, C.H., Leung, D.Y.C., Lam, K.M., 2006. Recent progress in CFD modelling of a wind field and pollutant transport in street canyons. Atmospheric Environment, vol. 40, pp. 5640-5658.
Lilly, D.K., 1992. A proposed modification of the Germano subgrid-scale closure method. Physics of Fluids, vol. 4, pp. 633-635.
Liu, C.-H., Barth, M.C., 2002. Large-eddy simulation of flow and scalar transport in a modeled street canyon. Journal of Applied Meteorology, vol. 41, pp. 660-673.
Liu, C.-H., Barth, M.C., Leung, D.Y.C., 2004. Large-eddy simulation of flow and pollutant transport in street canyons of different building-height-to-street-width ratios. Journal of Applied Meteorology, vol. 43, pp. 1410-1424.
Liu, C.-H., Leung, D.Y.C., 2008. Numerical study on the ozone formation inside street canyons using a chemistry box model. Journal of Environmental Sciences, vol. 20, pp. 832-837.
Liu, C.-H., Leung, D.Y.C., Barth, M.C., 2005. On the prediction of air and pollutant exchange rates in street canyons of different aspect ratios using large-eddy simulation. Atmospheric Environment, vol. 39, pp. 1567-1574.
Louka, P., Vachon, G., 2001. Thermal effects on the airflow in a street canyon - nantes ‘99 experimental results and model simulation. In: Proceedings of the Third International Conference on Urban Air Quality, Loutraki, Greece.
Madalozzo, D. M. S., Braun, A. L., Awruch. M A. Finite element simulation of non-isothermal pollutant dispersion in urban street canyons using shared memory parallelization. In: Proceedings of the 10th World Congress on Computational Mechanics (WCCM10), São Paulo, Brazil.
Meneveau, C., Lund, T.S., Cabot, W.H., 1996. A Lagrangian dynamic subgrid-scale model for turbulence. Journal of Fluid Mechanics, vol. 319, pp. 353-385.
Meroney, R.N, Pavageau, M., Rafailidis, S., Schatzmann, M., 1996. Study of line source characteristics for 2-D physical modelling of pollutant dispersion in street canyons. In: Journal of Wind Engineering and Industrial Aerodynamics, n. 62, p. 37–56.
Murakami, S., 1997. Current status and future trends in computational wind engineering. Journal of Wind Engineering and Industrial Aerodynamics, vols. 67&68, pp. 3-34.
Nicholson, S.E., 1975. A pollution model for street-level air. Atmospheric Environment, vol. 9, pp. 19-31.
Oke, T. R., 1988. Street design and urban canopy layer climate. Energy and Buildings, vol. 11, pp. 103-113.
Palmgren, F., Berkowicz, R., Hertel, O., Vignati, E., 1996. Effects of reduction in NOx on the NO2 levels in urban streets. Science of the Total Environment, vols. 189/190, pp. 409-415.
Pavageau, M., Schatzmann, M., 1999. Wind tunnel measurements of concentration fluctuations in an urban street canyon. Atmospheric Environment, vol. 33, pp. 3961-3971.
Piomelli, U., 2008. Wall-layer models for large-eddy simulations. Progress in Aerospace Science, vol. 44, pp. 437-466.
Popiolek, T. L., 2005. Análise de escoamentos incompressíveis utilizando simulação de grandes escalas e adaptação de malhas. D.Sc. Thesis, PPGEC/UFRGS, Porto Alegre, Brazil.
Reynolds, A.J., 1975. The prediction of turbulent prandtl and schmidt number. International Journal of Heat and Mass Transfer, vol. 18, pp. 1055-1069.

Sakakibara, Y., 1996. A numerical study of the effect of urban geometry upon the surface energy budget. Atmospheric Environment, vol. 30, pp. 487–496.
Salim, S. M., Buccolieri, R, Chan, A, Sabatino, S. D. Numerical simulation of atmospheric pollutant dispersion in na urban street canyon: Comparison between RANS and LES. Journal of Wind Engineering and Industrial Aerodynamics, vol. 99, pp. 103-113.
Santiago, J.L., Dejoan, A., Martilli, A., Martin, F., Pinelli, A., 2010. Comparison between large-eddy simulation and Reynolds-averaged Navier–Stokes computations for the MUST field experiment. Part I: Study of the flow for an incident wind directed perpendicularly to the front array of containers. Boundary-Layer Meteorology, vol. 135, pp. 109-132.
Shih, T.H., Liou, W.W., Shabbir, A., Zhu, J., 1995. A new k-ε eddy-viscosity model for high Reynolds numbers turbulent flows-model development and validation. Computers & Fluids, vol. 24, pp. 227-238.
Sini, J.-F., Anquetin, S., Mestayer, P.G., 1996. Pollutant dispersion and thermal effects in urban street canyons. Atmospheric Environment, vol. 30, pp. 2659-2677.
So, E.S.P., Chan, A.T.Y., Wong, A.Y.T., 2005. Large-eddy simulations of wind flow and pollutant dispersion in a street canyon. Atmospheric Environment, vol. 39, pp. 3573-3582.
Soulhac, L., Garbero, V., Salizzoni, P., Mejean, P., Perkins, R.J., 2009. Flow and dispersion in street canyons. Atmospheric Environment, vol. 43, pp. 2981-2996.
Smagorinsky, J., 1963. General circulation experiments with the primitive equations I. The basic experiment. Monthly Weather Review, vol. 91, pp. 99-164.
Tang, L.Q., Cheng, T., Tsang, T.T.H., 1995. Transient solutions for three-dimensional lid-driven cavity flows by least-squares finite element method. International Journal for Numerical Methods in Fluids, vol. 21, pp. 413-432.
Tominaga, Y., Stathopoulos, T., 2007. Turbulent Schmidt numbers for CFD analysis with various types of flowfield. Atmospheric Environment, vol. 41, pp. 8091-8099.
Tominaga, Y., Stathopoulos, T., 2010. Numerical simulation of dispersion around an isolated cubic building: model evaluation of RANS and LES. Building and Environment, vol. 45, pp. 2231-2239.
Tominaga, Y., Stathopoulos, T., 2011. CFD modeling of pollution dispersion in a street canyon: comparison between LES and RANS. Journal of Wind Engineering and Industrial Aerodynamics, vol. 99, pp. 340-348.
Uehara, K., Murakami, S., Oikawa, S., Wakamatsu, S., 2000. Wind tunnel experiments on how thermal stratification affects flow in and above urban street canyons. Atmospheric Environment, vol. 34, pp. 1553-1562.
Vardoulakis, S., Fisher, B.E., Pericleous, K., Gonzalez-Flesca, N., 2003. Modelling air quality in street canyons: A review. Atmospheric Environment, vol. 37, pp. 155-182.
Walton, A., Cheng, A.Y.S., Yeung, W.C., 2002. Large-eddy simulation of pollution dispersion in an urban street canyon. Part I: Comparison with field data. Atmospheric Environment, vol. 36, pp. 3601-3613.
Walton, A., Cheng, A.Y.S., 2002. Large-eddy simulation of pollution dispersion in an urban street canyon. Part II: Idealized canyon simulation. Atmospheric Environment, vol. 36, pp. 3615-3627.
Wilcox, D.C., 1988. Reassessment of the scale-determining equation for advanced turbulence models. AIAA Journal, vol. 26, pp. 1299-1310.
Xie, X., Huang, Z., Wang, J., Xie, Z., 2005. The impact of solar radiation and street layout on pollutant dispersion in street canyon. Building and Environment, vol. 40, pp. 201-212.
Xie, X., Liu, C-H., Leung, D.Y.C., Leung, M.K.H., 2006. Spatial distribution of traffic-related pollutant concentrations in street canyons. Atmospheric Environment, vol. 40, pp. 6396-6409.
Xie, S., Zhang, Y., Qi, L., Tang, X., 2003. Spatial distribution of traffic-related pollutant concentrations in street canyons. Atmospheric Environment, vol. 37, pp. 3213-3224.
Yakhot, V., Orszag, S.A., 1986. Renormalization group analysis of turbulence: I. Basic theory. Journal of Scientific Computing, vol. 1, pp. 1-51.
Yassin, M.F., Kellnerová, R., Janour, Z., 2008. Impact of street intersections on air quality in urban environment. Atmospheric Environment, vol. 42, pp. 4984-4963.